N6-methyladenosine RNA methylation is a novel epitranscriptomic regulator of excessive alcohol drinking and vulnerability to relapse

Riccardo Maccioni[1*], Irene Lorrai[1], Itzamar Torres[1], Roberta Puliga[1,2], Vez Repunte-Canonigo[1], Pietro Paolo Sanna[1*]

[1]Department of Immunology and Microbiology, The Scripps Research Institute, La Jolla, CA, USA 92037

[1,2]Department of Life and Environmental Sciences, University of Cagliari, Monserrato, Cagliari, Italy

*Correspondence:

rmaccioni@scripps.edu

psanna@scripps.edu

Abstract

While internal RNA modifications have been known for decades, the contribution of epitranscriptomics to alcohol use disorder (AUD) remains unexplored. Here we investigated, for the first time, the role of the most abundant mRNA modification, N6-methyladenosine (m^6A) in the regulation of alcohol drinking and alcohol mediated gene expression. The fat mass and obesity associated gene (FTO) plays a key role in erasing m^6A RNA methylation marks. We generated brain m^6A hypermethylated mice with selective deletion of FTO in neurons by crossing FTO-floxed mice (FTO-fl/fl) with the synapsin-1-CRE deleter line (Syn1-CRE). Neuronal FTO-deficient mice showed enhanced initial motivation for alcohol, achieved escalated (dependent) drinking more rapidly after repeated cycles of alcohol intoxication and were more susceptible to relapse to heavy drinking following a period of abstinence. Alcohol-naive neuronal FTO-deficient mice exhibited potentiated alcohol-induced anxiolytic and sedative effects and blunted anxiogenic responses, despite unaltered alcohol metabolism. We carried out RNA-Seq of enriched methylated RNA by immunoprecipitation (MeRIP) and RNA-Seq profiling of unenriched RNA to study alcohol's effect on the epitranscriptomic and transcriptional landscape. We observed that a history of alcohol intoxication induces robust RNA m^6A hypermethylation in the hippocampus and that FTO-deficiency markedly alters m^6A methylation and transcriptional dynamics. GSEA pathway analysis showed that neuronal FTO deficiency induces addiction-relevant pathways and alters monoaminergic and GABAergic neurotransmission, providing a molecular basis for the heightened vulnerability to alcohol abuse. Our findings demonstrate that neuronal m^6A RNA methylation is a novel regulator of excessive alcohol drinking and alcohol-dependent gene expression and its dysregulation may contribute to the pathogenesis AUD.

Introduction

More than 170 distinct chemical modifications have been identified across coding and non-coding mammalian RNAs comprising the “epitranscriptome” (1) and contributing to the regulation of RNA expression and metabolism (2-5). Akin to epigenetic regulation of DNA, these internal covalent RNA modifications influence its transcriptional efficiency, altering gene expression without changing the underlying genetic code (6-10). Among these, RNA methylation, particularly N6-methyladenosine (m^6A) in the mRNA, is the most abundant and conserved modification (11). Highly regulated mRNAs often contain m^6A residues, while mRNAs encoding housekeeping genes are less likely to be m^6A methylated (3, 12). m^6A mRNA modifications are found preferentially in the conserved motif DRACH (D = G/A/U, R = G/A, H = A/U/C) in 3’-UTRs and in proximity of the stop codons, and contribute to the regulation of its splicing, nuclear export, stability, and translation (7, 13-19). Multiple proteins are involved in the regulation of m^6A RNA methylation, acting as writers, erasers and readers resulting in dynamically regulation of m^6A methylation (8, 20). Among these proteins, the fat mass and obesity associated gene (FTO) plays a key role in erasing m^6A RNA methylation marks (21). While m^6A has been found in mRNAs from diverse tissue types, the brain has especially high levels of m^6A (22). RNA m^6A methylation in the brain modulates neuronal differentiation, synaptic plasticity, memory stabilization, and reward circuitry, and its dysregulation contributes to psychiatric disorders (22-24).

We observed that FTO deficiency enhances the initial motivation for alcohol, hastens the emergence of alcohol dependence, and increases relapse-like drinking during protracted withdrawal. We also observed a robust and unidirectional alcohol-mediated increase in m^6A methylation within the hippocampus of alcohol-dependent mice during acute withdrawal and that FTO deletion led to broad alterations of both m^6A RNA methylation and gene expression in both alcohol-naive and alcohol-dependent mice, particularly in genes related to monoaminergic and GABAergic neurotransmission, as well as in multiple addiction-related signaling pathways. Altogether, these results support a role for FTO and m^6A RNA methylation in excessive alcohol drinking and

indicate molecular mechanisms that likely contribute to the enhanced vulnerability of FTO-deficient mice to develop and maintain excessive drinking behavior.

Results

Deletion of neuronal FTO accelerates acquisition of alcohol drinking, onset of alcohol dependence and promotes relapse behavior

We bred FTO floxed mice (FTO-fl/fl) with the Synapsin 1 CRE deleter line (Syn1-CRE) to broadly and selectively delete FTO in neurons. We first measured initial preference for alcohol, followed by 4 weeks of non-dependent alcohol-drinking (Baseline, BL1 – BL4) with a 2 Bottle Choice (2BC) paradigm (Fig.1A). Alcohol-naive FTO-Syn1-CRE mice consumed significantly more alcohol than control FTO-fl/fl mice during their first exposure to alcohol (Fig.1 B). However, average drinking did not differ between the two genotypes over 4 weeks (Fig.1 C).

To assess the potential role of neuronal FTO in dependent drinking, we induced alcohol dependence by repeated cycles of alcohol vapor exposure with the Chronic Intermittent Ethanol paradigm coupled with 2 Bottle Choice (CIE-2BC). FTO-Syn1-CRE mice only required 2 cycles of CIE-2BC to achieve significantly escalated (dependent) alcohol drinking, while 3 cycles were required for FTO-fl/fl mice (Fig.1 D). Blood Alcohol Levels (BALs) did not differ between FTO-Syn1-CRE and FTO-fl/fl mice after vapor exposure, indicating that the two genotypes were exposed to equal amounts of alcohol vapors and that neuronal suppression of FTO does not impact alcohol metabolism (Supplementary Information, Supplementary Figure 1). We then tested the role of neuronal FTO in reinstatement behavior. To this end, alcohol withdrawal was induced in dependent FTO-Syn1-CRE and FTO-fl/fl mice by preventing alcohol access for 10 days (Fig.1 A). When mice were re-exposed to alcohol in the 2BC, FTO-Syn1-CRE mice consumed a statistically significant greater amount of alcohol than FTO-fl/fl mice (Fig.1 E). Finally, we analyzed the correlation between initial (first 2BC as alcohol-naive) and later (baseline, CIE-2BC and total) consumption of alcohol in the two genotypes. While in FTO-fl/fl mice

initial drinking showed a correlation with their subsequent drinking, no such association was observed in FTO-Syn1-CRE mice (Fig.1 F-H). Collectively, these results indicate that neuronal FTO deletion alters drinking trajectories and promote a more vulnerable phenotype characterized by enhanced early alcohol motivation, more rapid development of dependence, and increased relapse-like behavior.

Deletion of neuronal FTO potentiates alcohol-induced anxiolysis and prevents alcohol-induced anxiogenic response

We then evaluated the contribution of neuronal FTO to acute alcohol-induced anxiety manifestations in the Elevated Plus Maze (EPM) and Light and Dark Transition (LDT) tests (Fig.2 A). In the EPM, acute alcohol administration induced a stronger anxiolytic effect in FTO-Syn1-CRE mice, as indicated by a significantly higher percentage of time spent in the open arms than alcohol-treated FTO-fl/fl controls (Fig.2 B). As expected, significant alcohol-induced anxiolytic effects were present in both FTO-Syn1-CRE and FTO-fl/fl mice in both the time and entries in the open arms in comparison to saline-administered mice (Fig.2 B, C). No significant differences among FTO-fl/fl and FTO-Syn1-CRE mice were revealed upon saline administration in both parameters (Fig.2 B, C). Importantly, measures of total entries in both open and closed arms excluded alcohol-induced sedation in either genotype, while pointed to a higher degree of activity in FTO-Syn1-CRE than FTO-fl/fl mice (Fig.2 D). Conversely, alcohol induced anxiogenic responses in the LDT test in FTO-fl/fl that were not observed in FTO-Syn1-CRE, as indicated by the percentage of time spent in (Fig.2 E) and ambulation (Fig.2 F) in the light zone, which were drastically reduced in the control mice, but unchanged in FTO-deficient mice upon alcohol administration. Similarly to what observed in the EPM, we did not see any difference in mice that were administered saline before the test (Fig.2 E, F), and we observed a strong effect of genotype in mediating mice locomotor activity, with FTO-Syn1-CRE mice generally more active than FTO-fl/fl mice, in particular upon alcohol-treatment (Fig.2 G).

Deletion of neuronal FTO potentiates alcohol-induced sedative and hypnotic effects

Since alcohol-induced anxiolysis and sedation share overlapping mechanisms (25, 26), we also assessed FTO-fl/fl and FTO-Syn1-CRE mice in the Loss Of Righting Reflex (LORR) to evaluate alcohol-induced sedation and hypnosis (Fig.3 A). Sedation was rapidly induced by an acute injection of an intoxicating dose of alcohol (3.5 g/kg) in both genotypes (Fig.3 B). In keeping with the enhanced anxiolytic response to alcohol, FTO-Syn1-CRE also exhibited higher sensitivity to alcohol-induced hypnotic and sedative effects, as indicated by the significant increase in LORR duration (Fig. 3C). Measurement of BALs from blood samples collected at the moment of awakening and 2 hours after alcohol injection did not reveal any difference between FTO-fl/fl and FTO-Syn1-CRE mice, ruling out differences in alcohol metabolism between the genotypes (Fig.3 D).

Alcohol dependence increases RNA m^{6}A methylation and differentially alters m^{6}A methylation of neuronal and signaling pathways under neuronal FTO suppression.

We carried out MeRIP (Methylated RNA Immunoprecipitation) to investigate the effect of alcohol on m^{6}A RNA methylation. poly-A selected RNA was extracted from the hippocampus of alcohol-naive and alcohol-dependent FTO-fl/fl and FTO-Syn1-CRE mice after 24 hours of withdrawal from the last exposure to alcohol vapors (Fig.4 A-G). Principal component analysis (PCA) of m^{6}A methylation profiles revealed clear separation across genotypes and treatment conditions, indicating robust effects of neuronal-FTO deletion and alcohol treatment (Fig.4 A). Alcohol-dependence induced a dramatic unidirectional change in the m^{6}A methylation pattern in control FTO-fl/fl mice, with 441 significantly m^{6}A hypermethylated transcripts (and only 2 hypomethylated) in comparison to their alcohol-naive littermates. The number of differentially regulated transcripts revealed by the comparison between alcohol-naive and alcohol-dependent FTO-Syn1-CRE mice was considerably smaller (54 m^{6}A hypermethylated, 1

hypomethylated transcripts by alcohol) (Fig.4 C), which could be due to the higher level of m^6A methylation of FTO-deficient mice. In fact, comparison between alcohol-naive FTO-fl/fl mice and naive-FTO-Syn1-CRE revealed 763 m^6A hypermethylated transcripts and 1 m^6A hypomethylated transcript in FTO-deficient mice (Fig.4 E). Comparison between alcohol-dependent FTO-fl/fl and alcohol-dependent FTO-Syn1-CRE mice revealed 57 (53 hypermethylated, 4 hypomethylated) differently m^6A regulated transcripts in FTO-deficient mice (Fig.4 D). The comparison between alcohol-naive FTO-fl/fl and alcohol-dependent FTO-Syn1-CRE mice revealed the most dramatic difference, with 1,203 hypermethylated transcripts (Fig.3 E). Quality control (QC) and metagene distribution plots are available in the Supplementary Information (Supplementary Figure 2).

We then used the Gene Set Enrichment Analysis (GSEA) algorithm to identify molecular pathways differently regulated by alcohol in FTO-fl/fl and FTO-Syn1-CRE mice. The analysis revealed 151 upregulated pathways in alcohol-dependent FTO-Syn1-CRE mice in comparison to alcohol-dependent FTO-fl/fl mice. Moreover, we identified 231 (38 down, 193 up) pathways altered by alcohol in FTO-fl/fl mice and 204 (39 down, 165 up) in FTO-Syn1-CRE, 269 (43 down, 226 up) comparing alcohol-naive FTO-fl/fl and alcohol-dependent FTO-Syn1-CRE and 258 (49 down, 209 up) comparing naive FTO-fl/fl with alcohol-naive FTO-Syn1-CRE.

As m^6A RNA methylation is enriched in neurons and FTO was selectively deleted in neurons, we filtered the shared pathways with high neuronal relevance and evaluated the alterations in signaling dynamics (Fig.3 G). Interestingly, we observed a marked general upregulation of pathways involved in neurotransmitter transport and release in alcohol-naive FTO-Syn1-CRE. Many signaling pathways involved in synaptic plasticity and neurogenesis, like the MAPK-ERK (27, 28), WNT signaling (29, 30), and SMAD signaling (31) also resulted significantly upregulated. Interestingly, the comparison between alcohol-dependent FTO-Syn1-CRE and FTO-fl/fl showed that while synaptic dynamics are globally downregulated in FTO-deficient mice, signaling pathways seem

overall enhanced. Finally, both alcohol-naive and alcohol-dependent FTO-Syn1-CRE mice showed a general upregulation of apoptotic dynamics but interestingly, also a strong reduction of the TNFα pro-inflammatory pathway. Differentially m^6A methylated transcripts were also involved in cytoskeleton dynamics and cell motility, membrane trafficking and ER-Golgi functionality, RNA metabolism, transcription and epigenetic regulation, metabolism, as well as immune and inflammatory responses and neuronal dynamics.

Neuronal FTO loss amplifies alcohol withdrawal driven transcriptional responses and alters synaptic and intracellular signaling pathways

RNA-Seq analysis was also carried out from the hippocampus of alcohol naive and alcohol-dependent FTO-fl/fl and FTO-Syn1-CRE mice after 24 hours of withdrawal (Fig.5 A-G). Principal component analysis (PCA) revealed clear separation across genotypes and treatment conditions, indicating robust effects of neuronal-FTO deletion and alcohol treatment (Fig.5 A). Importantly, a history of alcohol dependence had a more pronounced effect on FTO-Syn1-CRE than in FTO fl/fl control. The comparison between alcohol-naive and alcohol-dependent FTO fl/fl control mice revealed 662 differently expressed genes (Fig.5 B), while 976 were revealed comparing naive and alcohol-dependent FTO-Syn1-CRE littermates (Fig.5 C) and 192 differently expressed genes were found comparing alcohol-dependent FTO-fl/fl and FTO-Syn1-CRE mice, with FTO being one of the most significantly down-regulated genes in FTO-Syn1-CRE mice (Fig.5 D). Similarly, FTO was among the most down-regulated genes in the comparison between naive FTO-Syn1-CRE and FTO-fl/fl mice, which revealed 1034 differentially expressed genes (Fig.5 E). As expected, comparing alcohol-dependent FTO-Syn1-CRE mice with naive FTO-fl/fl mice revealed the greatest effect, with 2133 significantly differentially expressed genes (Fig.5 F).

We then used the Gene Set Enrichment Analysis (GSEA) algorithm to identify molecular pathways differently regulated by alcohol in FTO-fl/fl and FTO-Syn1-CRE mice. Alcohol differentially regulated 310 pathways (299 up, 11 down) in FTO-fl/fl and 245 (227 up, 18 down) in FTO-Syn1-CRE mice. Importantly, 108 pathways were differentially regulated

between alcohol-dependent FTO-fl/fl and FTO-Syn1-CRE mice, with 22 up and 86 down in FTO-deficient mice. The comparison between naive FTO-fl/fl and FTO-Syn1-CRE mice revealed 202 modified pathways, with 63 up- and 139 downregulated in FTO-deficient mice. Finally, 216 differentially pathways were revealed comparing alcohol-dependent FTO- Syn1-CRE and naive FTO-fl/fl, with 161 up- and 55 downregulated pathways in FTO-Syn1-CRE mice.

These differentially regulated pathways are involved in neuronal and synaptic dynamics, cytoskeleton organization, stress and damage response, metabolism and bioenergetics, transcription and epigenetics, as well as immune and inflammatory responses. We then filtered the shared pathways with high neuronal relevance and evaluated the alterations in signaling dynamics in the same way we did for the differentially regulated pathways derived from the GSEA of our m^6A dataset (Fig.5 G). Importantly, pathways related to GABAergic synapses and transmission were strongly and significantly downregulated in alcohol-dependent FTO-Syn1-CRE mice in comparison to alcohol-dependent FTO-fl/fl after 24 hours of withdrawal. In support to what disclosed by the GSEA of our m^6A dataset, FTO-deletion induced significant upregulation in pathways involved in neurotransmitter release and transmission. Accordingly, pathways related to the release of monoamines and catecholamines, as well as in neurotransmitter receptors responsiveness resulted strongly upregulated in FTO-Syn1-CRE mice. FTO-deficiency induced a significant upregulation of addiction-related signaling pathways, like those involved in the regulation of MAPK-ERK signaling (27, 28), in keeping with the GSEA pathway analysis of the MeRIP data, and the neuropeptide signaling pathway (32). Notably, these same addiction-related pathways resulted upregulated in alcohol-dependent FTO-fl/fl when compared to their naive littermates.

Discussion

Alcohol use disorder (AUD) is one of the most consequential mental disorders worldwide and is a leading risk factor for global disease burden and premature death

(33, 34). Thus, there is a pressing need to better understand its complexity to identify new and more effective druggable targets (35). While the role of canonical epigenetic gene regulation in the pathogenesis of AUD has been extensively explored (36-38), the role of epitranscriptomic modifications remain uncharacterized. Neurons have especially high levels of m^6A, which regulate key processes underling synaptic plasticity, learning and memory formation (21, 22, 39-41). RNA m^6A methylation is a reversible modification, and its removal is mediated by FTO (42), making it a key regulator of gene expression states (5). Here we provide the first evidence of a critical functional role of m^6A methylation and its demethylase FTO in the effects of alcohol and in the vulnerability to develop AUD.

We generated mice with neuronal m^6A hypermethylation through selective neuronal knockout of FTO, and tested their alcohol sensitivity, alcohol intake and alcohol-dependence. Selective neuronal deletion of FTO resulted in heightened initial motivational response to alcohol in alcohol-naive mice. The transition to addiction involves neuroplasticity and neuroadaptations that begin with changes in the mesolimbic dopamine system followed by broad neuroadaptations in other limbic circuits (43). FTO knock down in dopaminergic neurons has been shown to potentiate cocaine-induced positive reinforcement and associative learning in conditioned place preference (44). Learning processes driven by positive or negative reinforce are implicated in drinking trajectories as, for instance, early alcohol consumption is a predictor of subsequent drinking behavior in rodents (45, 46). We observed an absence of correlation in mice lacking neuronal FTO unlike their control counterpart, which suggests that FTO regulates the translation of early reinforcing experiences into heavy drinking patterns, and its absence renders FTO-deficient mice more susceptible to the development of dependence. In humans, FTO genetic variants increase susceptibility to obesity through altered sensitivity and learning from negative outcomes (47).

Our observation that neuronal FTO deficient mice required fewer alcohol exposures to achieve alcohol dependence-associated escalated drinking and exhibited enhanced relapse-like behavior suggests a predisposition to accelerated and heightened alcohol-induced neuroadaptive and plastic processes. This is also supported by GSEA pathway

analysis of our RNA-Seq gene expression and MeRIP findings, which revealed widespread dysregulation of synaptic signaling and neurotransmission-related pathways, particularly monoaminergic and GABA neurotransmission in mice with neuronal FTO-deficiency. In addition, multiple signaling cascades known to govern synaptic plasticity, neurogenesis, and addiction-relevant neuroadaptations, such as MAPK-ERK signaling (27, 28), neuropeptide signaling (32), neurotrophic pathways (48, 49) and WNT-signaling (29, 30) were also significantly upregulated, supporting a greater predisposition to maladaptive synaptic remodeling in the absence of FTO. These alterations might constitute the molecular basis of the increased vulnerability of mice with neuronal FTO-deficiency, in keeping with previous reports implicating FTO and m^6A in synaptic plasticity and memory formation (39, 41, 42, 50).

We observed a critical potentiation of alcohol-induced locomotor responses in our FTO-deficient mice. Alcohol-induced hyperactivity is dopamine dependent (51). Increased locomotor response to cocaine was also observed in mice with FTO deficiency in dopaminergic neurons (44), as well enhanced locomotor response to novelty (52). Interestingly, our GSEA pathway analysis revealed significant upregulation of catecholamine and monoamine transport and secretion pathways in alcohol-naive FTO-deficient mice.

Mice with neuronal deficiency of FTO were also more susceptible to relapse to heavy drinking following a period of abstinence. Withdrawal from chronic alcohol decreases GABA neurotransmission (53). Insufficient GABAergic inhibition may result in withdrawal manifestations such as anxiety, hyperexcitability, insomnia, and seizures which may contribute to alcohol-seeking behavior (54). GSEA analysis of our RNA-Seq dataset revealed a significant downregulation of GABAergic signaling pathways in alcohol-dependent FTO-deficient mice during alcohol withdrawal compared to control mice.

FTO deletion elicited m^6A methylation changes in transcripts crucial for $GABA_A$ receptors localization and functionality during alcohol withdrawal. The most hypermethylated transcript in alcohol-dependent control mice was *Arhgef7*. *Arhgef7* localizes to both presynaptic sites and in the post synaptic density, where it maintains the surface expression of $GABA_A$ receptors at inhibitory synapses, ensuring proper

inhibitory neurotransmission (55). Paradoxically, alcohol-dependent FTO-deficient mice displayed significantly lower m^6A methylation levels of *Arhgef7* compared to alcohol-dependent controls. Furthermore, the *Nbea* transcript was highly methylated in both alcohol-dependent and naive FTO-deficient mice in comparison to control littermates. *Nbea* is an essential component of inhibitory synapses and regulates receptor trafficking and $GABA_A$ receptors internalization (56). In further support, hypermethylated transcripts in alcohol-dependent FTO-deficient mice are *Camk2a*, that phosphorylates $GABA_A$ receptors and potentiates GABA currents (57) and *Erc2*, which has been identified as a structural component of $GABA_A$ receptors (58). Alterations in $GABA_A$ receptors and GABA dynamics are suggested also by the different phenotype of FTO-deficient mice in the anxiety and sedative responses to acute alcohol. We observed that genetic inhibition of FTO markedly potentiates alcohol-induced anxiolysis and completely blunted anxiogenic responses. The subjective way in which individuals emotionally experience early alcohol exposures is a critical determinant for later AUD risk (59-61) and drinking to cope with anxiety or for tension reduction is consistently associated with greater risk of problematic use, underscoring the reinforcing impact of anxiolysis itself (62-64).

$GABA_A$ receptors also mediate alcohol's sedative and hypnotic properties (25, 26). In agreement, we also report increased sensitivity to alcohol-induced hypnosis in FTO-deficient mice, that could act as a limiting factor to excessive consumption, in keeping with the absence of significant effects of FTO-deficiency on alcohol intake during chronic heavy exposure. In support, FTO and m^6A RNA methylation have been implicated in the regulation of stress response, anxiety and depression (65, 66) and its knockdown has been shown to increase the expression of $GABA_A$ receptor subunits (67), key molecular targets of anxiety manifestations of typical anxiolytic drugs, as well as alcohol (25, 68, 69). Increased $GABA_A$ receptor-mediated response to acute alcohol may underlie the enhanced alcohol-induced anxiolysis and sedative response that we observed. GABA-hypersensitivity would also explain the exacerbation of the molecular signatures of alcohol-induced GABAergic withdrawal (53, 54, 70, 71) that we observed in alcohol-dependent FTO-deficient mice, as well as their propension to relapse.

In summary, our findings identify RNA m^6A methylation as a critical contributor to the maladaptive neuroplasticity that underlies excessive alcohol drinking and vulnerability to relapse that characterize alcohol addiction (72). The present behavioral, m^6A-profiling and transcriptomic data, suggest that RNA m^6A methylation may increase individual vulnerability to AUD due to predisposition to neuroadaptive changes and neurotransmitter dysregulation that contribute to enhance the initial motivational response to alcohol, accelerate the onset of dependence and aggravate relapse behavior. The involvement of m^6A dysregulation also in depression and stress responses, which are associated with AUD vulnerability (73) suggest that targeting m^6A-regulated pathways may represent a promising direction for therapeutic intervention.

Methods

Animals

All experimental procedures were approved by the Institutional Animal Care and Use Committee of The Scripps research Institute and performed in accordance with the Association for Assessment and Accreditation of Laboratory Animal Care. *FTO*$^{flox/flox}$ mice were generously provided by Dr. Clemens (Johns Hopkins University). To generate brain neuronal specific *FTO* deletion, *FTO*$^{flox/flox}$ mice were crossed with *Syn1-Cre* mice (JAX 003966) to generate *FTO*$^{+/flox}$/*Tg(Syn1-Cre)* mice, which were then crossed to *FTO*$^{flox/flox}$ mice to generate the experimental *FTO-fl/fl* and FTO-Syn1-CRE mice. Adult male C57BL/6J mice (The Jackson Laboratories, USA) were used for the experimental procedures involving FTO pharmacological inhibition with Meclofenamic Acid. Animals were housed in a climate-controlled vivarium on a 12 h/12 h reverse light/dark cycle (lights on 9:00 AM) and provided with free access to water and food (7012 Teklad LM-485 Rodent Diet, inotive, IN, USA) throughout the study.

Drugs and Treatments

The FTO inhibitor Meclofenamic Acid (MA) (HY-B1320, MedChemExpress) was prepared fresh everyday by suspension into Tween 80 (5% w/v) and at a concentration

of 5 mg/kg (74). Mice were intraperitoneally (IP) injected daily with MA (10mL/kg) for 4 months before the behavioral procedures began. On experimental day, MA was administered 30 minutes before the beginning of the test (EPM, LORR).

2-bottle choice paradigm and Chronic intermittent access (CIE) to alcohol vapors

Male FTO-fl/fl and FTO-Syn1-CRE mice were singly housed and exposed to the conventional 2-bottle alcohol [15% (v/v)] vs water choice (2BC) paradigm for 4 weeks (5 weekly 2h sessions) to measure initial alcohol intake in naive mice and obtain a baseline of alcohol-intake. Alcohol and water consumption were recorded by weighing the bottles before and after the drinking session. Subsequently, mice were exposed to intermittent ethanol vapor (CIE, 16h ON, 9h OFF) to induce escalated-dependent drinking. Statistically significant escalation was defined by $p<0.05$ vs the last week of baseline alcohol intake. Before being exposed to alcohol vapors, mice were injected IP with a solution of alcohol (1.5 g/kg, 15% w/v in saline) containing 68.1 mg/kg pyrazole and immediately placed into alcohol vapor chambers (La Jolla Ethanol Research, CA, USA) to reach target Blood Alcohol Levels (BALs) of 150–200 mg/dL. Seventy-two hours following removal from the chambers, mice received access to water versus 15% v/v alcohol for 2 hours, and again over the next 4 days. The following week, mice were re-exposed to the alcohol vapor/control conditions and again tested for 2BC drinking for 5 days. 4 total alcohol vapor cycles followed by 2BC were carried out. After the last cycle, mice were prevented from accessing alcohol for a total of 10 days to induce withdrawal and were then tested acutely with a 2BC test to measure reinstatement-like behavior. Mice were then re-exposed to a week of vapors and euthanized 24h after the last exposure. Body weight was taken every 4–6 days throughout the 2BC sessions and daily during the vapor exposure bouts. Food and water were available ad libitum, and mice were always group-housed except during the alcohol-drinking sessions.

Blood alcohol levels (BALs)

BALs were determined by a conventional oxygen-rate alcohol analyzer (Analox Instruments, Atlanta, GA). The reaction is based on alcohol oxidation of alcohol oxidase in the presence of molecular oxygen (ethanol + O_2 -> acetaldehyde + H_2O_2). The rate of oxygen consumption is directly proportional to the alcohol concentration. Blood was collected from tail tip, and BALs were collected along the CIE-2BC procedure and after the loss of righting reflex procedures.

Elevated Plus Maze and Light and Dark Transition Test

The Elevated Plus Maze (EPM) procedures were conducted according to our previous studies (75, 76). The EPM consisted of a central platform (5×5 cm, W×L) and two open arms (5×30 cm, W×L) aligned perpendicularly to two closed transparent arms (5×30 cm, W×L) at the height of 40 cm from the ground. FTO-fl/fl and FTO-Syn1-CRE mice were administered with alcohol (1.5 g/kg) or saline and tested 5 minutes later. The spontaneous activity of mice was automatically recorded for 5 min. Data were calculated as the percentage of time spent in the open arms (*time spent in the open arms divided by the time spent in the open arms* + *time spent in the closed arms*) and as the percentage of open arm entries (*number of entries into the open arms divided by the number of entries into the open arms* + *number of entries into the closed arms*). The total number of entries was measured and report as a measure of activity and to exclude sedation. The analysis was automatically performed by ANY-Maze software. Similarly, a separate cohort of FTO-fl/fl and FTO-Syn1-CRE mice was administered with alcohol (1.5 g/kg) or saline and tested at the 5 minutes later. The spontaneous activity of mice was automatically recorded for 10 min. Data were calculated as the percentage of time spent in the Light Zone, as well as the percentage of locomotor activity in the Light Zone. The total locomotor activity was measured and report as a measure of activity and to exclude sedation. The analysis was automatic as the Light and Dark arena was provided with infrared photo beams (Med Associates, USA).

mRNA isolation and m^6A-modified RNA immunoprecipitation (MeRIP)

After 24h of withdrawal, total RNA was extracted from dissected hippocampi of FTO-fl/fl and FTO-Syn1-CRE mice with RNEasy kit (Qiagen) and poly-A selected with Dynabeads Oligo(dT)25 (Thermo Fisher Scientific) following manufacturer's instructions. Poly-A enriched RNA was recovered by ethanol precipitation overnight, fragmented using RNA Fragmentation Reagents (Thermo Fisher Scientific) and ethanol precipitation overnight. An aliquot of fragmented RNA was set aside serving as input or control for RNA sequencing. Twenty µg of fragmented RNAs were denatured at 75°C for 5 min, cooled on ice for 3 min, and then incubated for 2h at 4°C with 3 µg of pre-equilibrated anti-m^6A (Synaptic Systems), which was pre-immobilized to M-270 Epoxy using the Dynabeads Antibody Coupling kit (Thermo Fisher Scientific) for easy capture of the m^6A-modified RNA in subsequent elution with a Proteinase K-containing buffer. Eluate with the anti-m^6A captured RNA was extracted by phenol/CHCl3 followed by ethanol precipitation.

EpiPlex™ m6A methylation encoding and pulldown

m6A methylation detection was performed using AlidaBio's EpiPlex™ RNA Mod Encoding Kit (P/N 100124) using 1 µg purified total RNA isolated from mouse brain tissue as input. Sequencing libraries were prepared following kit instructions as previously written (77). In brief, RNA sample and spike-in controls were fragmented and ligated to an Illumina P7 adapter. Modified fragments were enriched on magnetic beads coated with modification-specific binders and corresponding Illumina P5 adapters, comprising a modification barcode (MBC) to capture and encode the RNA modification identity during reverse transcription, then PCR amplified using the EpiPlex™ Unique Dual Index Primer Kit (P/N 296001). A portion of the sample bypasses enrichment to provide a solution control library with RNA-Seq information. Ribosomal RNA was removed using the SEQuoia RiboDepletion Kit (Bio-Rad, P/N 17006487), and final libraries were prepared through additional PCR cycles. Paired-end libraries were sequenced to ~50 - 80M reads on an Illumina NovaSeq X with the 10B (200 Cycle) Reagent Kit (P/N 20085595).

EpiScout™ m6A peak calling and analysis

EpiPlex™ sequencing reads were processed using AlidaBio's EpiScout™ v1.2 pipeline. The latest EpiScout™ software can be found in DockerHub (https://hub.docker.com/r/alidabio/episcout). Briefly, raw read quality was assessed using FastQC (2). Reads with length <30, mean quality <30, or NNN content >10% were discarded. Clean reads were then mapped to the mouse genome (GRCm39) and the EpiPlex™ internal spike-in control using STAR v2.7.11a (78). Genome mapped reads were split by MBC and deduplicated according to MBC and Unique Molecular Identifier (UMI) barcodes using samtools v1.20 (79) and custom Python and C++ libraries.

Peak calling was performed using a Hidden Markov Model (HMM) based on the ratio of enriched and solution control read pileups, internal spike-in standard curve, and sequencing depth ratio between enrichment and solution control libraries. Peak quality was assessed using random forest model log-probabilities, represented as a PHRED scale q-score (random_forest_q). Peaks were annotated using the GRCm39 gtf file and a custom bedtools script (80).

EpiScout™ differential m6A peak identification analysis

Significant increases and decreases in m6A methylation were identified using the EpiScout™ pipeline. Briefly, peak intersection sets for each condition were identified using bedtools, requiring at least one replicate per condition to contain a peak that passes the random forest filter criteria. A count profile matrix from the union of peak regions between conditions was then generated, normalizing for library sizes, then extreme values using Trimmed Mean of M-values method (81).

Briefly, differential m6A enrichment was assessed through the condition:sample interaction coefficient of a Poisson Generalized Linear Model, using an additional coefficient accounting for background transcript expression. p-values adjusted for multiple testing using the Benjamini-Hochberg false discovery rate procedure. Log_2 fold changes were calculated as the difference between normalized enrichment ratios

across conditions. Separately, differential transcript expression analysis was performed on the EpiPlex solution control library using DESeq2 (82). Significance for differential analysis was determined using adjusted $p < 0.05$.

Gene Set Enrichment Analysis (GSEA) of m6A methylation and RNA-Seq expression profiles

Functional pathways relating to m6A methylation and expression were identified using GSEA (83, 84). Briefly, count matrices for m6A and RNA-Seq profiles were provided as input to the GSEA command-line tool. Mouse Molecular Signature Database (MSigDB) gene sets MH, M1, M2, M3, M5, M7, and M8 were used (85). Pathways with $p < 0.05$ were reported. All the neuronal and signaling pathways were filtered from all the shared pathways with $p <0.05$ in at least one of the comparisons

Figure Captions

Fig.1 Genetic deletion of FTO in neurons results in enhanced initial motivation for alcohol, hastened alcohol dependence, and increased relapse-like drinking. (A) Timeline of experimental procedures. **(B)** Alcohol intake (g/kg) measured after the first 2BC in FTO-fl/fl and FTO-Syn1-CRE mice. *p<0.05 by unpaired t-test. **(C)** Average weekly alcohol intake (g/kg) of 4 weeks of baseline measurements (BL1-4) in FTO-fl/fl and FTO-Syn1-CRE mice. **(D)** Alcohol intake (g/kg) during CIE-2BC in FTO-fl/fl and FTO-Syn1-CRE mice. *p<0.05, **p<0.01 vs BL4 by Two-way repeated measure (RM) ANOVA followed by Tukey's post hoc *vs* BL 4. **(E)** Alcohol intake (g/kg) during the single 2BC conducted after 10 days of withdrawal. p<0.05 by unpaired t-test. **(F-H)** Pearson's correlation analysis between the initial alcohol intake from the first 2BC and the average of the non-dependent alcohol intake **(F)**, the average alcohol consumption during the CIE-2BC cycles **(G)** and the average of total alcohol consumption along the whole procedure **(H)**. *p<0.05, **p<0.01.

Fig.2 Genetic deletion of FTO in neurons increases alcohol-induced anxiolysis and anxiogenic responses. (A) FTO-fl/fl and FTO-Syn1-CRE mice were assessed at the Elevated Plus Maze (EPM) and the Light and Dark Transition Test (LTD) after 5 minutes from a single acute IP administration of alcohol (1.5 g/kg). **(B, C)** Percentage of time and entries in the open arms of FTO-fl/fl and FTO-Syn1-CRE mice with and without alcohol treatment. *p<0.05, **p<0.01, ***p<0.001, ****p<0.0001 by Two-way ANOVA followed by Tukey's post hoc). **(D)** Total entries in the open arms of FTO-fl/fl and FTO-Syn1-CRE mice. *p<0.05 by Two-way ANOVA followed by Tukey's post hoc. **(E, F)** Percentage of time **(E)** and ambulation **(F)** in the Light Zone (LZ) of FTO-fl/fl and FTO-Syn1-CRE mice with and without alcohol treatment. *p<0.05, **p<0.01, by Two-way ANOVA followed by Tukey's post hoc). **(D)** Total locomotor activity of FTO-fl/fl and FTO-Syn1-CRE mice. **p<0.01, ****p<0.0001 by Two-way ANOVA followed by Tukey's post hoc.

Fig. 3 Increased sensitivity of the intoxicating effect of alcohol in mice with neuronal FTO deficiency. Alcohol (3.5 g/kg, IP) induced Loss Of Righting Reflex (LORR) in FTO-fl/fl and FTO-Syn1-CRE mice **(A)**. FTO-Syn1-CRE mice showed unchanged time to sedation (B) but higher duration of sedation **(C)**. *p<0.05 by unpaired t-test. No differences between the two genotypes were observed in BALs were observed **(D)**. As expected, BALs at the 2H time point were lower than the ones at the Recovery Of Righting Reflex (RORR) **(D)**. **p<0.05 by Two-way RM ANOVA followed by Tukey's post hoc test.

Fig. 4 Identification and functional pathway analysis of differentially m6A methylated transcripts by MeRIP. A) Principal Component Analysis (PCA) of enriched m6A modification signal detected by the EpiPlex™ assay binned by gene-body regions. Genotype and treatment replicates are indicated by color: alcohol-naive -FTO-fl/fl (blue), alcohol-dependent FTO-fl/fl (green), alcohol-naive-FTO-Syn1-CRE (orange), alcohol-dependent FTO-Syn1-CRE (red). **B-F)** Volcano plots of differentially m6A methylated peaks. Transcript regions with significant increase or decrease in m6A methylation were identified by EpiScout™ software (FDR-corrected p-value < 0.05) **G)** Heatmap of neuronal and signaling pathways enrichment analysis. NES (Normalized Enrichment Scores) of differentially m6A methylated transcripts are shown. Select pathways with NOM p-value < 0.05 in at least one comparison are shown. Pathways related to cell signaling are labelled in orange, and pathways relating to neuronal dynamics are labeled in blue.

Fig. 5 Identification and functional pathway analysis of differentially expressed transcripts by RNA-Seq.

A) Principal Component Analysis (PCA) of RNA expression detected the RNA-Seq channel of the EpiPlex™ platform. Genotype and treatment replicates are indicated by color: alcohol-naive-FTO-fl/fl (blue), alcohol-dependent FTO-fl/fl (green), alcohol-naive-FTO-Syn1-CRE (orange), alcohol-dependent FTO-Syn1-CRE (red). **B-F)** Volcano plots of differentially expressed transcripts. Transcripts with significantly increased and decreased expression were identified using DEseq2 (FDR-corrected p-value < 0.05). **G)** Heatmap of pathway enrichment analysis. NES (Normalized Enrichment Scores) of differentially expressed transcripts are shown. Select pathways with NOM p-value < 0.05 in at least one comparison are shown. Pathways related to cell signaling are labelled in orange, and pathways relating to neuronal dynamics are labeled in blue.

Figure 1

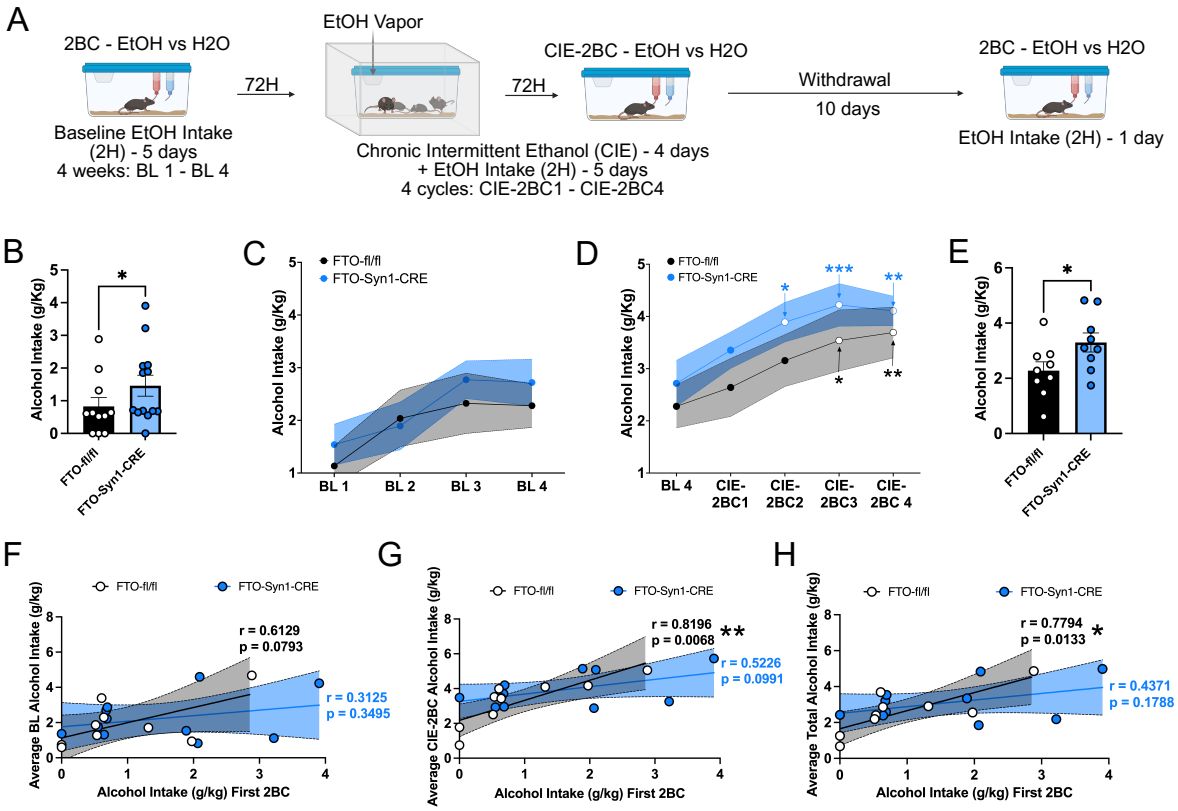
A
2BC - EtOH vs H2O
Baseline EtOH Intake (2H) - 5 days
4 weeks: BL 1 - BL 4
72H
EtOH Vapor
Chronic Intermittent Ethanol (CIE) - 4 days
+ EtOH Intake (2H) - 5 days
4 cycles: CIE-2BC1 - CIE-2BC4
72H
CIE-2BC - EtOH vs H2O
Withdrawal
10 days
2BC - EtOH vs H2O
EtOH Intake (2H) - 1 day
B
Alcohol Intake (g/Kg)
FTO-fl/fl
FTO-Syn1-CRE
C
FTO-fl/fl
FTO-Syn1-CRE
Alcohol Intake (g/Kg)
BL 1
BL 2
BL 3
BL 4
D
FTO-fl/fl
FTO-Syn1-CRE
Alcohol Intake (g/Kg)
BL 4
CIE-2BC1
CIE-2BC2
CIE-2BC3
CIE-2BC 4
E
Alcohol Intake (g/Kg)
FTO-fl/fl
FTO-Syn1-CRE
F
FTO-fl/fl
FTO-Syn1-CRE
r = 0.6129
p = 0.0793
r = 0.3125
p = 0.3495
Average BL Alcohol Intake (g/kg)
Alcohol Intake (g/kg) First 2BC
G
FTO-fl/fl
FTO-Syn1-CRE
r = 0.8196
p = 0.0068
r = 0.5226
p = 0.0991
Average CIE-2BC Alcohol Intake (g/kg)
Alcohol Intake (g/kg) First 2BC
H
FTO-fl/fl
FTO-Syn1-CRE
r = 0.7794
p = 0.0133
r = 0.4371
p = 0.1788
Average Total Alcohol Intake (g/kg)
Alcohol Intake (g/kg) First 2BC

Figure 2

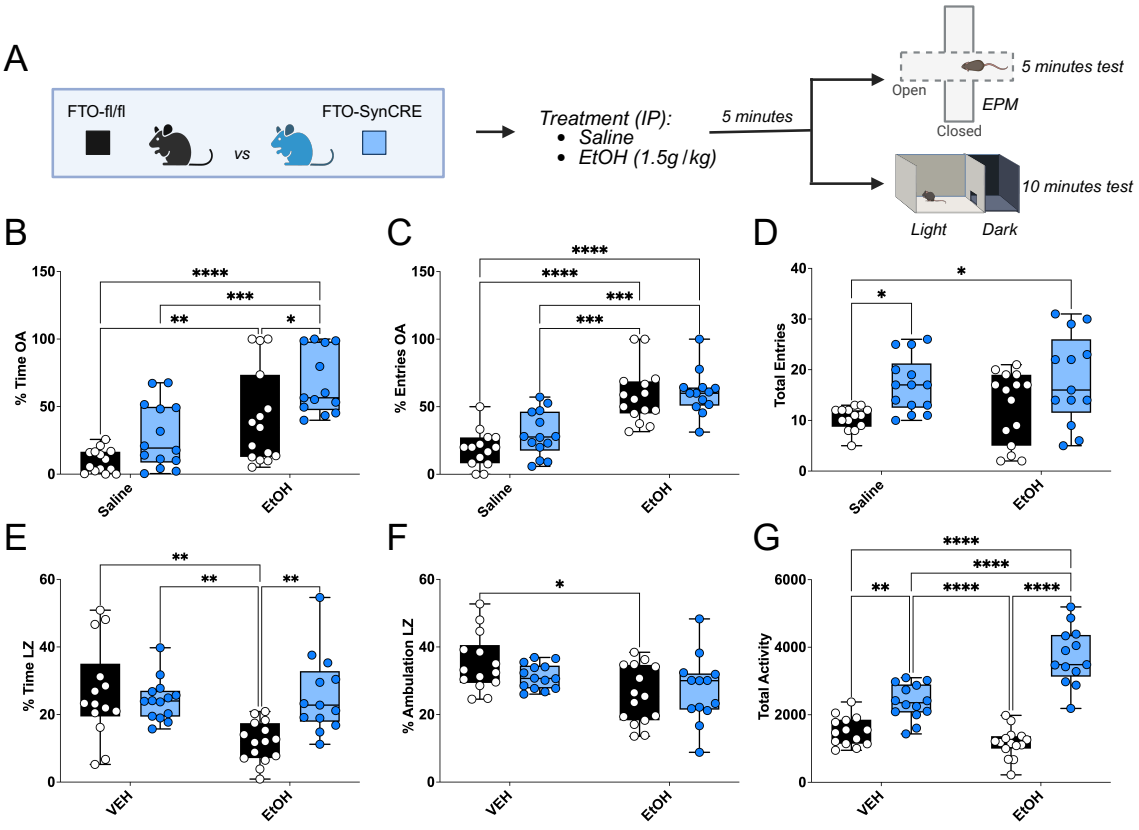
A
FTO-fl/fl
vs
FTO-SynCRE
Treatment (IP):
Saline
EtOH (1.5g/kg)
5 minutes
5 minutes test
Open
EPM
Closed
10 minutes test
Light
Dark
B
% Time OA
Saline
EtOH
C
% Entries OA
D
Total Entries
E
% Time LZ
VEH
F
% Ambulation LZ
G
Total Activity

Figure 3

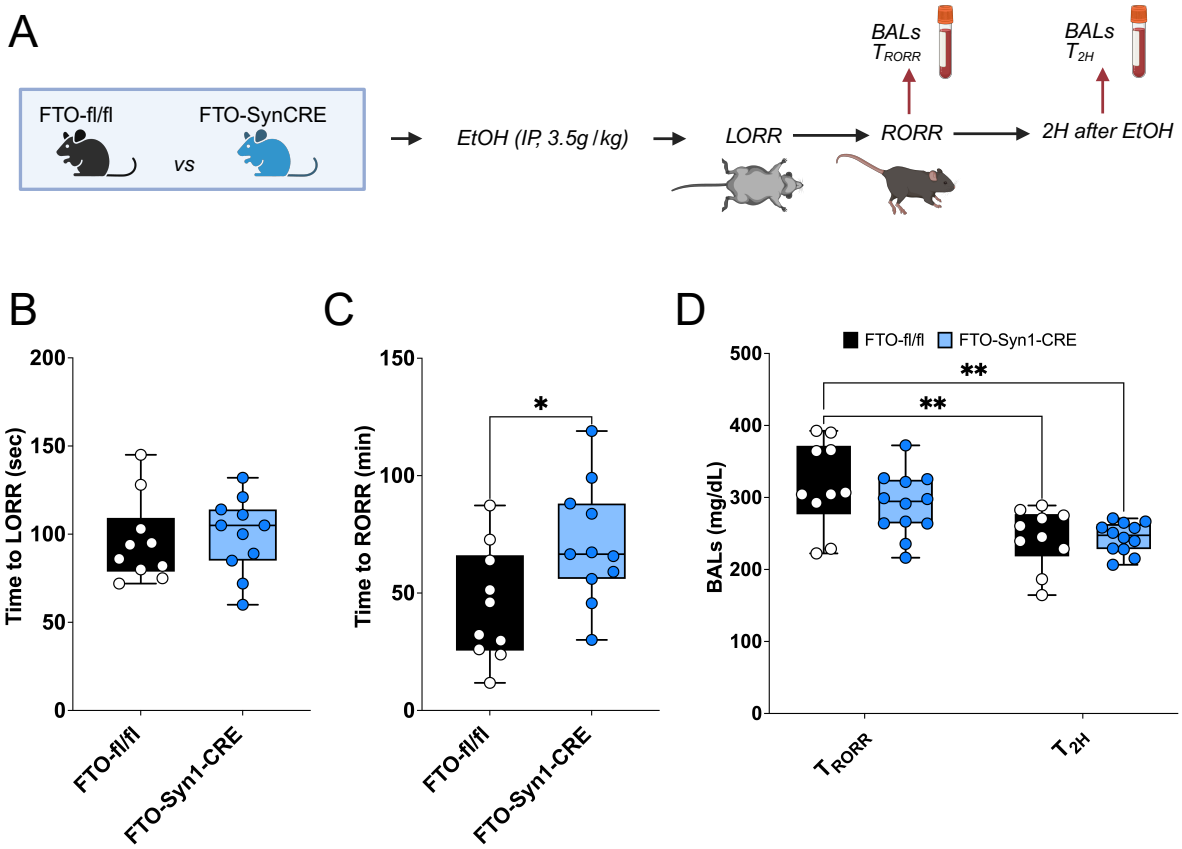
A
FTO-fl/fl
FTO-SynCRE
vs
EtOH (IP, 3.5g /kg)
LORR
RORR
2H after EtOH
BALs
T RORR
BALs
T 2H
B
Time to LORR (sec)
200
150
100
50
0
FTO-fl/fl
FTO-Syn1-CRE
C
Time to RORR (min)
150
100
50
0
*
FTO-fl/fl
FTO-Syn1-CRE
D
FTO-fl/fl
FTO-Syn1-CRE
BALs (mg/dL)
500
400
300
200
100
0
**
**
T RORR
T 2H

Figure 4

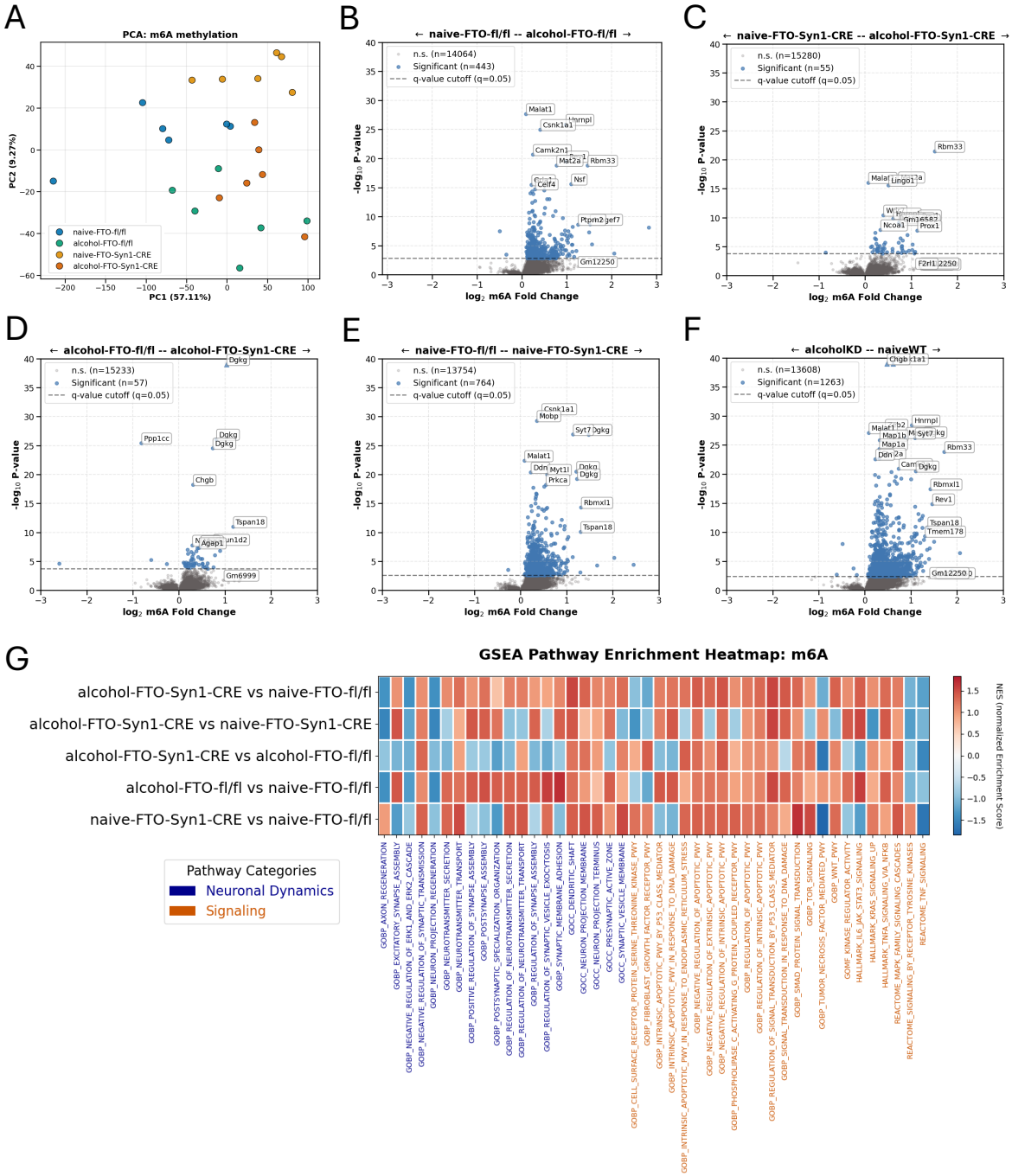
A
PCA: m6A methylation
PC2 (9.27%)
PC1 (57.11%)
naive-FTO-fl/fl
alcohol-FTO-fl/fl
naive-FTO-Syn1-CRE
alcohol-FTO-Syn1-CRE
B
← naive-FTO-fl/fl -- alcohol-FTO-fl/fl →
n.s. (n=14064)
Significant (n=443)
q-value cutoff (q=0.05)
-log10 P-value
log2 m6A Fold Change
C
← naive-FTO-Syn1-CRE -- alcohol-FTO-Syn1-CRE →
n.s. (n=15280)
Significant (n=55)
q-value cutoff (q=0.05)
D
← alcohol-FTO-fl/fl -- alcohol-FTO-Syn1-CRE →
n.s. (n=15233)
Significant (n=57)
q-value cutoff (q=0.05)
E
← naive-FTO-fl/fl -- naive-FTO-Syn1-CRE →
n.s. (n=13754)
Significant (n=764)
q-value cutoff (q=0.05)
F
← alcoholKD -- naiveWT →
n.s. (n=13608)
Significant (n=1263)
q-value cutoff (q=0.05)
G
GSEA Pathway Enrichment Heatmap: m6A
alcohol-FTO-Syn1-CRE vs naive-FTO-fl/fl
alcohol-FTO-Syn1-CRE vs naive-FTO-Syn1-CRE
alcohol-FTO-Syn1-CRE vs alcohol-FTO-fl/fl
alcohol-FTO-fl/fl vs naive-FTO-fl/fl
naive-FTO-Syn1-CRE vs naive-FTO-fl/fl
NES (normalized Enrichment Score)
Pathway Categories
Neuronal Dynamics
Signaling

Figure 5

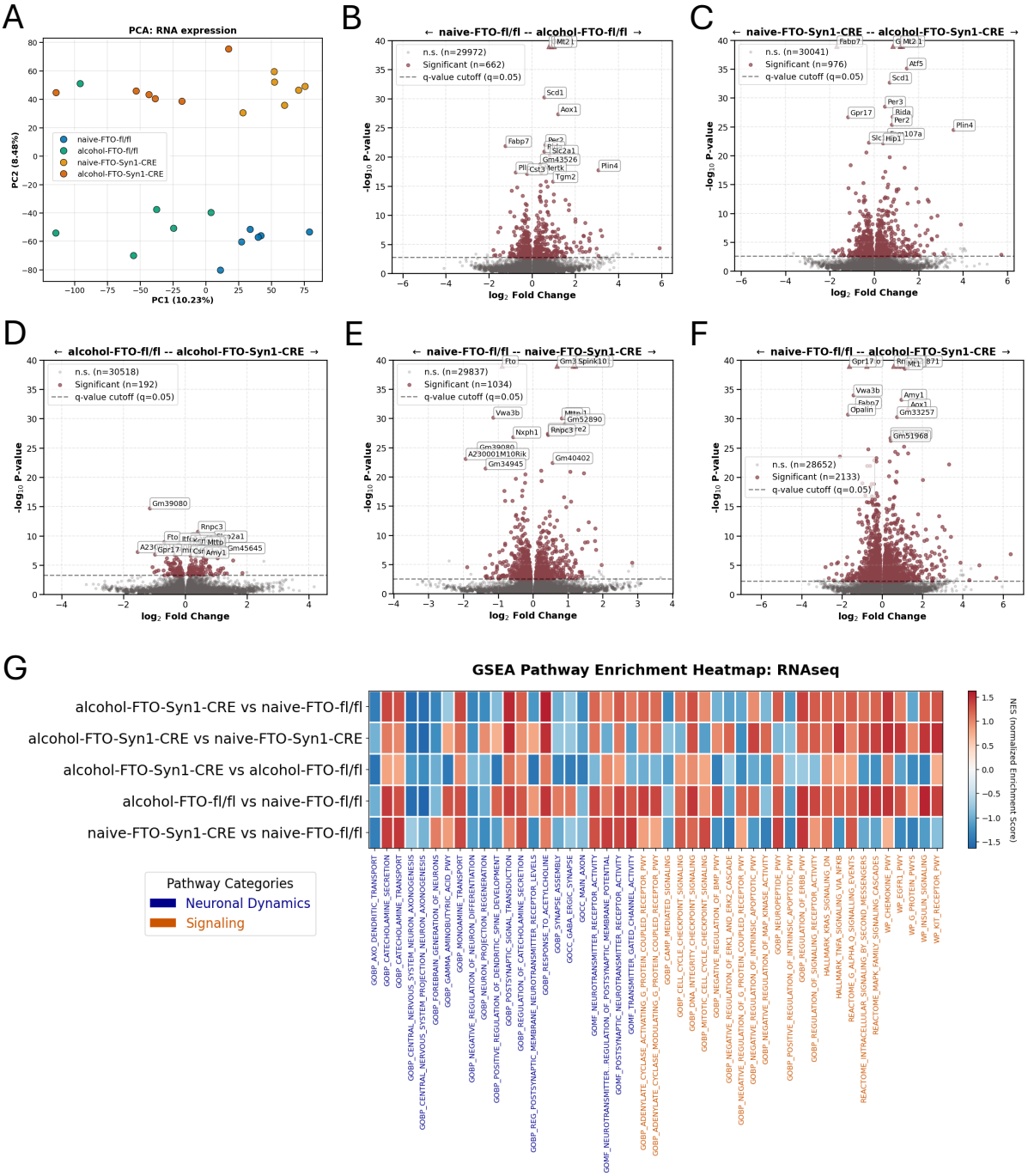
A
PCA: RNA expression
naive-FTO-fl/fl
alcohol-FTO-fl/fl
naive-FTO-Syn1-CRE
alcohol-FTO-Syn1-CRE
PC1 (10.23%)
PC2 (8.48%)
B
← naive-FTO-fl/fl -- alcohol-FTO-fl/fl →
n.s. (n=29972)
Significant (n=662)
q-value cutoff (q=0.05)
log2 Fold Change
-log10 P-value
C
← naive-FTO-Syn1-CRE -- alcohol-FTO-Syn1-CRE →
n.s. (n=30041)
Significant (n=976)
q-value cutoff (q=0.05)
D
← alcohol-FTO-fl/fl -- alcohol-FTO-Syn1-CRE →
n.s. (n=30518)
Significant (n=192)
q-value cutoff (q=0.05)
E
← naive-FTO-fl/fl -- naive-FTO-Syn1-CRE →
n.s. (n=29837)
Significant (n=1034)
q-value cutoff (q=0.05)
F
← naive-FTO-fl/fl -- alcohol-FTO-Syn1-CRE →
n.s. (n=28652)
Significant (n=2133)
q-value cutoff (q=0.05)
G
GSEA Pathway Enrichment Heatmap: RNAseq
alcohol-FTO-Syn1-CRE vs naive-FTO-fl/fl
alcohol-FTO-Syn1-CRE vs naive-FTO-Syn1-CRE
alcohol-FTO-Syn1-CRE vs alcohol-FTO-fl/fl
alcohol-FTO-fl/fl vs naive-FTO-fl/fl
naive-FTO-Syn1-CRE vs naive-FTO-fl/fl
NES (normalized Enrichment Score)
Pathway Categories
Neuronal Dynamics
Signaling

Acknowledgments

This work was supported by NIH Grant AA021667; IL was partially supported by training grant # T32 AA007456.

References

1. Boccaletto P, Stefaniak F, Ray A, Cappannini A, Mukherjee S, Purta E, Kurkowska M, Shirvanizadeh N, Destefanis E, Groza P, Avsar G, Romitelli A, Pir P, Dassi E, Conticello SG, Aguilo F, Bujnicki JM. 2022. MODOMICS: a database of RNA modification pathways. 2021 update. Nucleic Acids Res 50:D231-D235.
2. Li S, Mason CE. 2014. The pivotal regulatory landscape of RNA modifications. Annu Rev Genomics Hum Genet 15:127-50.
3. Meyer KD, Jaffrey SR. 2016. Expanding the diversity of DNA base modifications with N(6)-methyldeoxyadenosine. Genome Biol 17:5.
4. Roundtree IA, Evans ME, Pan T, He C. 2017. Dynamic RNA Modifications in Gene Expression Regulation. Cell 169:1187-1200.
5. Cerneckis J, Ming GL, Song H, He C, Shi Y. 2024. The rise of epitranscriptomics: recent developments and future directions. Trends Pharmacol Sci 45:24-38.
6. Dominissini D, Moshitch-Moshkovitz S, Schwartz S, Salmon-Divon M, Ungar L, Osenberg S, Cesarkas K, Jacob-Hirsch J, Amariglio N, Kupiec M, Sorek R, Rechavi G. 2012. Topology of the human and mouse m6A RNA methylomes revealed by m6A-seq. Nature 485:201-6.
7. Meyer KD, Saletore Y, Zumbo P, Elemento O, Mason CE, Jaffrey SR. 2012. Comprehensive analysis of mRNA methylation reveals enrichment in 3' UTRs and near stop codons. Cell 149:1635-46.
8. Fu Y, Dominissini D, Rechavi G, He C. 2014. Gene expression regulation mediated through reversible m(6)A RNA methylation. Nat Rev Genet 15:293-306.
9. Cao G, Li HB, Yin Z, Flavell RA. 2016. Recent advances in dynamic m6A RNA modification. Open Biol 6:160003.
10. Ke S, Pandya-Jones A, Saito Y, Fak JJ, Vagbo CB, Geula S, Hanna JH, Black DL, Darnell JE, Jr., Darnell RB. 2017. m6A mRNA modifications are deposited in nascent pre-mRNA and are not required for splicing but do specify cytoplasmic turnover. Genes Dev 31:990-1006.
11. Jiang X, Liu B, Nie Z, Duan L, Xiong Q, Jin Z, Yang C, Chen Y. 2021. The role of m6A modification in the biological functions and diseases. Signal Transduct Target Ther 6:74.
12. Yue Y, Liu J, He C. 2015. RNA N6-methyladenosine methylation in post-transcriptional gene expression regulation. Genes Dev 29:1343-55.

13. Liu N, Dai Q, Zheng G, He C, Parisien M, Pan T. 2015. N(6)-methyladenosine-dependent RNA structural switches regulate RNA-protein interactions. Nature 518:560-4.
14. Wei W, Ji X, Guo X, Ji S. 2017. Regulatory Role of N6 -methyladenosine (m6 A) Methylation in RNA Processing and Human Diseases. J Cell Biochem 118:2534-2543.
15. Wang X, Lu Z, Gomez A, Hon GC, Yue Y, Han D, Fu Y, Parisien M, Dai Q, Jia G, Ren B, Pan T, He C. 2014. N6-methyladenosine-dependent regulation of messenger RNA stability. Nature 505:117-20.
16. Wang X, Zhao BS, Roundtree IA, Lu Z, Han D, Ma H, Weng X, Chen K, Shi H, He C. 2015. N(6)-methyladenosine Modulates Messenger RNA Translation Efficiency. Cell 161:1388-99.
17. Xiao W, Adhikari S, Dahal U, Chen YS, Hao YJ, Sun BF, Sun HY, Li A, Ping XL, Lai WY, Wang X, Ma HL, Huang CM, Yang Y, Huang N, Jiang GB, Wang HL, Zhou Q, Wang XJ, Zhao YL, Yang YG. 2016. Nuclear m(6)A Reader YTHDC1 Regulates mRNA Splicing. Mol Cell 61:507-19.
18. Xu C, Wang X, Liu K, Roundtree IA, Tempel W, Li Y, Lu Z, He C, Min J. 2014. Structural basis for selective binding of m6A RNA by the YTHDC1 YTH domain. Nat Chem Biol 10:927-9.
19. Boulias K, Greer EL. 2023. Biological roles of adenine methylation in RNA. Nat Rev Genet 24:143-160.
20. Shi H, Wei J, He C. 2019. Where, When, and How: Context-Dependent Functions of RNA Methylation Writers, Readers, and Erasers. Mol Cell 74:640-650.
21. Jia G, Fu Y, Zhao X, Dai Q, Zheng G, Yang Y, Yi C, Lindahl T, Pan T, Yang YG, He C. 2011. N6-methyladenosine in nuclear RNA is a major substrate of the obesity-associated FTO. Nat Chem Biol 7:885-7.
22. Satterlee JS, Basanta-Sanchez M, Blanco S, Li JB, Meyer K, Pollock J, Sadri-Vakili G, Rybak-Wolf A. 2014. Novel RNA modifications in the nervous system: form and function. J Neurosci 34:15170-7.
23. Ngo AL, Nguyen L, Gharavi Alkhansari N, Zhang H. 2025. m(6)A RNA Methylation in Psychiatric Disorders: An Emerging Epitranscriptomic Axis. Epigenomes 9.
24. Chang R, Huang Z, Zhao S, Zou J, Li Y, Tan S. 2022. Emerging Roles of FTO in Neuropsychiatric Disorders. Biomed Res Int 2022:2677312.
25. Davies M. 2003. The role of GABAA receptors in mediating the effects of alcohol in the central nervous system. J Psychiatry Neurosci 28:263-74.
26. Lobo IA, Harris RA. 2008. GABA(A) receptors and alcohol. Pharmacol Biochem Behav 90:90-4.
27. Sanna PP, Simpson C, Lutjens R, Koob G. 2002. ERK regulation in chronic ethanol exposure and withdrawal. Brain Res 948:186-91.
28. Sun WL, Quizon PM, Zhu J. 2016. Molecular Mechanism: ERK Signaling, Drug Addiction, and Behavioral Effects. Prog Mol Biol Transl Sci 137:1-40.
29. Cuesta S, Severin MJ, Batuecas J, Rosso SB, Pacchioni AM. 2017. Wnt/beta-catenin pathway in the prefrontal cortex is required for cocaine-induced neuroadaptations. Addict Biol 22:933-945.

30. Gawlinski D, Gawlinska K, Frankowska M, Filip M. 2022. Cocaine and Its Abstinence Condition Modulate Striatal and Hippocampal Wnt Signaling in a Male Rat Model of Drug Self-Administration. Int J Mol Sci 23.
31. Jovanovic VM, Salti A, Tilleman H, Zega K, Jukic MM, Zou H, Friedel RH, Prakash N, Blaess S, Edenhofer F, Brodski C. 2018. BMP/SMAD Pathway Promotes Neurogenesis of Midbrain Dopaminergic Neurons In Vivo and in Human Induced Pluripotent and Neural Stem Cells. J Neurosci 38:1662-1676.
32. Natividad LA, Buczynski MW, McClatchy DB, Yates JR, 3rd. 2018. From Synapse to Function: A Perspective on the Role of Neuroproteomics in Elucidating Mechanisms of Drug Addiction. Proteomes 6.
33. Collaborators GBDA. 2018. Alcohol use and burden for 195 countries and territories, 1990-2016: a systematic analysis for the Global Burden of Disease Study 2016. Lancet 392:1015-1035.
34. Collaborators GBDRF. 2020. Global burden of 87 risk factors in 204 countries and territories, 1990-2019: a systematic analysis for the Global Burden of Disease Study 2019. Lancet 396:1223-1249.
35. Litten RZ, Falk DE, Ryan ML, Fertig J, Leggio L. 2020. Five Priority Areas for Improving Medications Development for Alcohol Use Disorder and Promoting Their Routine Use in Clinical Practice. Alcohol Clin Exp Res 44:23-35.
36. Krishnan HR, Sakharkar AJ, Teppen TL, Berkel TD, Pandey SC. 2014. The epigenetic landscape of alcoholism. Int Rev Neurobiol 115:75-116.
37. Zhou H, Gelernter J. 2024. Human genetics and epigenetics of alcohol use disorder. J Clin Invest 134.
38. Pandey SC, Bohnsack JP. 2020. Alcohol Makes Its Epigenetic Marks. Cell Metab 31:213-214.
39. Li J, Yang X, Qi Z, Sang Y, Liu Y, Xu B, Liu W, Xu Z, Deng Y. 2019. The role of mRNA m(6)A methylation in the nervous system. Cell Biosci 9:66.
40. Zhang Z, Wang M, Xie D, Huang Z, Zhang L, Yang Y, Ma D, Li W, Zhou Q, Yang YG, Wang XJ. 2018. METTL3-mediated N(6)-methyladenosine mRNA modification enhances long-term memory consolidation. Cell Res 28:1050-1061.
41. Walters BJ, Mercaldo V, Gillon CJ, Yip M, Neve RL, Boyce FM, Frankland PW, Josselyn SA. 2017. The Role of The RNA Demethylase FTO (Fat Mass and Obesity-Associated) and mRNA Methylation in Hippocampal Memory Formation. Neuropsychopharmacology 42:1502-1510.
42. Shi H, Zhang X, Weng YL, Lu Z, Liu Y, Lu Z, Li J, Hao P, Zhang Y, Zhang F, Wu Y, Delgado JY, Su Y, Patel MJ, Cao X, Shen B, Huang X, Ming GL, Zhuang X, Song H, He C, Zhou T. 2018. m(6)A facilitates hippocampus-dependent learning and memory through YTHDF1. Nature 563:249-253.
43. Koob GF, Volkow ND. 2010. Neurocircuitry of addiction. Neuropsychopharmacology 35:217-38.
44. Hess ME, Hess S, Meyer KD, Verhagen LA, Koch L, Bronneke HS, Dietrich MO, Jordan SD, Saletore Y, Elemento O, Belgardt BF, Franz T, Horvath TL, Ruther U, Jaffrey SR, Kloppenburg P, Bruning JC. 2013. The fat mass and obesity associated gene (Fto) regulates activity of the dopaminergic midbrain circuitry. Nat Neurosci 16:1042-8.

45. Schramm-Sapyta NL, Kingsley MA, Rezvani AH, Propst K, Swartzwelder HS, Kuhn CM. 2008. Early ethanol consumption predicts relapse-like behavior in adolescent male rats. Alcohol Clin Exp Res 32:754-62.
46. Grisel JE, Beasley JB, Bertram EC, Decker BE, Duan CA, Etuma M, Hand A, Locklear MN, Whitmire MP. 2014. Initial subjective reward: single-exposure conditioned place preference to alcohol in mice. Front Neurosci 8:345.
47. Sevgi M, Rigoux L, Kuhn AB, Mauer J, Schilbach L, Hess ME, Gruendler TO, Ullsperger M, Stephan KE, Bruning JC, Tittgemeyer M. 2015. An Obesity-Predisposing Variant of the FTO Gene Regulates D2R-Dependent Reward Learning. J Neurosci 35:12584-92.
48. Bolanos CA, Nestler EJ. 2004. Neurotrophic mechanisms in drug addiction. Neuromolecular Med 5:69-83.
49. Russo SJ, Mazei-Robison MS, Ables JL, Nestler EJ. 2009. Neurotrophic factors and structural plasticity in addiction. Neuropharmacology 56 Suppl 1:73-82.
50. Mitsuhashi H, Nagy C. 2023. Potential Roles of m6A and FTO in Synaptic Connectivity and Major Depressive Disorder. Int J Mol Sci 24.
51. Phillips TJ, Shen EH. 1996. Neurochemical bases of locomotion and ethanol stimulant effects. Int Rev Neurobiol 39:243-82.
52. Ruud J, Alber J, Tokarska A, Engstrom Ruud L, Nolte H, Biglari N, Lippert R, Lautenschlager A, Cieslak PE, Szumiec L, Hess ME, Bronneke HS, Kruger M, Nissbrandt H, Korotkova T, Silberberg G, Rodriguez Parkitna J, Bruning JC. 2019. The Fat Mass and Obesity-Associated Protein (FTO) Regulates Locomotor Responses to Novelty via D2R Medium Spiny Neurons. Cell Rep 27:3182-3198 e9.
53. Dharavath RN, Pina-Leblanc C, Tang VM, Sloan ME, Nikolova YS, Pangarov P, Ruocco AC, Shield K, Voineskos D, Blumberger DM, Boileau I, Bozinoff N, Gerretsen P, Vieira E, Melamed OC, Sibille E, Quilty LC, Prevot TD. 2023. GABAergic signaling in alcohol use disorder and withdrawal: pathological involvement and therapeutic potential. Front Neural Circuits 17:1218737.
54. Liang J, Olsen RW. 2014. Alcohol use disorders and current pharmacological therapies: the role of GABA(A) receptors. Acta Pharmacol Sin 35:981-93.
55. Smith KR, Davenport EC, Wei J, Li X, Pathania M, Vaccaro V, Yan Z, Kittler JT. 2014. GIT1 and betaPIX are essential for GABA(A) receptor synaptic stability and inhibitory neurotransmission. Cell Rep 9:298-310.
56. Lutzenkirchen FP, Zhu Y, Maric HM, Boeck DS, Gromova KV, Kneussel M. 2024. Neurobeachin regulates receptor downscaling at GABAergic inhibitory synapses in a protein kinase A-dependent manner. Commun Biol 7:1635.
57. Houston CM, He Q, Smart TG. 2009. CaMKII phosphorylation of the GABA(A) receptor: receptor subtype- and synapse-specific modulation. J Physiol 587:2115-25.
58. Choi C, Smalley JL, Lemons AHS, Ren Q, Bope CE, Dengler JS, Davies PA, Moss SJ. 2022. Analyzing the mechanisms that facilitate the subtype-specific assembly of gamma-aminobutyric acid type A receptors. Front Mol Neurosci 15:1017404.
59. Ray LA, Mackillop J, Monti PM. 2010. Subjective responses to alcohol consumption as endophenotypes: advancing behavioral genetics in etiological and treatment models of alcoholism. Subst Use Misuse 45:1742-65.

60. Lewis MJ, June HL. 1990. Neurobehavioral studies of ethanol reward and activation. Alcohol 7:213-9.
61. Schuckit MA, Smith TL. 1996. An 8-year follow-up of 450 sons of alcoholic and control subjects. Arch Gen Psychiatry 53:202-10.
62. Dvorak RD, Stevenson BL, Kilwein TM, Sargent EM, Dunn ME, Leary AV, Kramer MP. 2018. Tension reduction and affect regulation: An examination of mood indices on drinking and non-drinking days among university student drinkers. Exp Clin Psychopharmacol 26:377-390.
63. Young RM, Oei TP, Knight RG. 1990. The tension reduction hypothesis revisited: an alcohol expectancy perspective. Br J Addict 85:31-40.
64. Kushner MG, Sher KJ, Wood MD, Wood PK. 1994. Anxiety and drinking behavior: moderating effects of tension-reduction alcohol outcome expectancies. Alcohol Clin Exp Res 18:852-60.
65. Sun L, Ma L, Zhang H, Cao Y, Wang C, Hou N, Huang N, von Deneen KM, Zhao C, Shi Y, Pan Y, Wang M, Ji G, Nie Y. 2019. Fto Deficiency Reduces Anxiety- and Depression-Like Behaviors in Mice via Alterations in Gut Microbiota. Theranostics 9:721-733.
66. Engel M, Eggert C, Kaplick PM, Eder M, Roh S, Tietze L, Namendorf C, Arloth J, Weber P, Rex-Haffner M, Geula S, Jakovcevski M, Hanna JH, Leshkowitz D, Uhr M, Wotjak CT, Schmidt MV, Deussing JM, Binder EB, Chen A. 2018. The Role of m(6)A/m-RNA Methylation in Stress Response Regulation. Neuron 99:389-403 e9.
67. Yang X, Qi Z, Yang H, Li J, Liu Y, Sang Y, Li M, Du X, Wang H, Liu B, Xu B, Liu W, Xu Z, Deng Y. 2022. The m(6)A mRNA demethylase FTO regulates GnRH secretion in Mn-induced precocious puberty. Mol Cell Endocrinol 542:111523.
68. Sigel E, Steinmann ME. 2012. Structure, function, and modulation of GABA(A) receptors. J Biol Chem 287:40224-31.
69. Low K, Crestani F, Keist R, Benke D, Brunig I, Benson JA, Fritschy JM, Rulicke T, Bluethmann H, Mohler H, Rudolph U. 2000. Molecular and neuronal substrate for the selective attenuation of anxiety. Science 290:131-4.
70. Sanna E, Mostallino MC, Busonero F, Talani G, Tranquilli S, Mameli M, Spiga S, Follesa P, Biggio G. 2003. Changes in GABA(A) receptor gene expression associated with selective alterations in receptor function and pharmacology after ethanol withdrawal. J Neurosci 23:11711-24.
71. Calixto E. 2016. GABA withdrawal syndrome: GABAA receptor, synapse, neurobiological implications and analogies with other abstinences. Neuroscience 313:57-72.
72. Koob GF. 2014. Neurocircuitry of alcohol addiction: synthesis from animal models. Handb Clin Neurol 125:33-54.
73. Castillo-Carniglia A, Keyes KM, Hasin DS, Cerda M. 2019. Psychiatric comorbidities in alcohol use disorder. Lancet Psychiatry 6:1068-1080.
74. Chang R, Zhu S, Peng J, Lang Z, Zhou X, Liao H, Zou J, Zeng P, Tan S. 2023. The hippocampal FTO-BDNF-TrkB pathway is required for novel object recognition memory reconsolidation in mice. Transl Psychiatry 13:349.
75. Sethi MK, Maccioni R, Hogan JD, Kawamura T, Repunte-Canonigo V, Chen J, Zaia J, Sanna PP. 2024. Comprehensive Glycomic and Proteomic Analysis of Mouse

Striatum and Lateral Hypothalamus Following Repeated Exposures to Cocaine or Methamphetamine. Mol Cell Proteomics 23:100803.
76. Maccioni R, Cottiglia F, Maccioni E, Talani G, Sanna E, Bassareo V, Kasture SB, Acquas E. 2021. The biologically active compound of Withania somnifera (L.) Dunal, docosanyl ferulate, is endowed with potent anxiolytic properties but devoid of typical benzodiazepine-like side effects. J Psychopharmacol 35:1277-1284.
77. Yoshida A, Song Y, Takaine H, Song S, Konishi N, Hwang-Fu YH, Johnson Z, Ura K, Sassa A. 2025. Epitranscriptome-wide profiling identifies RNA editing events regulated by ADAR1 that are associated with DNA repair mechanisms in human TK6 cells. Front Genet 16:1663827.
78. Dobin A, Davis CA, Schlesinger F, Drenkow J, Zaleski C, Jha S, Batut P, Chaisson M, Gingeras TR. 2013. STAR: ultrafast universal RNA-seq aligner. Bioinformatics 29:15-21.
79. Danecek P, Bonfield JK, Liddle J, Marshall J, Ohan V, Pollard MO, Whitwham A, Keane T, McCarthy SA, Davies RM, Li H. 2021. Twelve years of SAMtools and BCFtools. Gigascience 10.
80. Quinlan AR, Hall IM. 2010. BEDTools: a flexible suite of utilities for comparing genomic features. Bioinformatics 26:841-2.
81. Robinson MD, Oshlack A. 2010. A scaling normalization method for differential expression analysis of RNA-seq data. Genome Biol 11:R25.
82. Love MI, Huber W, Anders S. 2014. Moderated estimation of fold change and dispersion for RNA-seq data with DESeq2. Genome Biol 15:550.
83. Subramanian A, Tamayo P, Mootha VK, Mukherjee S, Ebert BL, Gillette MA, Paulovich A, Pomeroy SL, Golub TR, Lander ES, Mesirov JP. 2005. Gene set enrichment analysis: a knowledge-based approach for interpreting genome-wide expression profiles. Proc Natl Acad Sci U S A 102:15545-50.
84. Mootha VK, Lindgren CM, Eriksson KF, Subramanian A, Sihag S, Lehar J, Puigserver P, Carlsson E, Ridderstrale M, Laurila E, Houstis N, Daly MJ, Patterson N, Mesirov JP, Golub TR, Tamayo P, Spiegelman B, Lander ES, Hirschhorn JN, Altshuler D, Groop LC. 2003. PGC-1alpha-responsive genes involved in oxidative phosphorylation are coordinately downregulated in human diabetes. Nat Genet 34:267-73.
85. Castanza AS, Recla JM, Eby D, Thorvaldsdottir H, Bult CJ, Mesirov JP. 2023. Extending support for mouse data in the Molecular Signatures Database (MSigDB). Nat Methods 20:1619-1620.